ap

Asian Journal of Physics
Vol. 29, Nos 10-12 (2020) 853-862
Available on: www.asianjournalofphysics.com

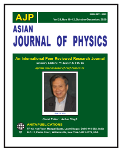

Scaling up low resolution noisy images in a multi-aperture imaging system

Suhita Tawade[1],Suresh Panchal[1], Rajeev Kumar[3] and Unnikrishnan Gopinathan[1,2]
[1]*Department of Applied Physics, Defence Institute of Advanced Technology, Girinagar, Pune-411 025, India*
[2] *Instruments Research & Development Establishment, Raipur Road, Dehradun-248 008, India*
[3]*Defence Institute of Advanced Technology, Girinagar, Pune-411 025, India*

This article is dedicated to Prof FTS Yu for his significant contributions to Optics and Optical information Processing

A multi-aperture imaging camera is a computational imaging camera that uses a micro-lens array to achieve a smaller system volume as compared to a conventional camera without compromising the resolution and field of view. A micro-lens array with each micro-lens shifted from a regular grid form multiple, low-resolution images. A robust signal processing algorithm to generate a high-resolution image from the multiple low-resolution images generated by the micro-lens array forms an essential component of such a computational camera. In this paper, a robust image super-resolution algorithm for a multi-aperture imaging system using ℓ_1 regularization is developed. The image formation in multiple imaging channels is modelled mathematically by taking into account the various degradations in the image formation process. The proposed super-resolution algorithm has two steps. In the first step the degradations in each imaging channel is corrected by solving the inverse problem of reconstructing the high-resolution image from a set of low-resolution images which is an ill-posed problem. The inverse problem is formulated as an optimization problem with a ℓ_1 regularization term which is solved as an unconstrained problem with FISTA algorithm and as a constrained optimization problem with SALSA algorithm. In the second step, the images from the multiple channels are combined to generate a high-resolution image after correcting for sub-pixel shifts between the images thereby effectively achieving a sampling on a high-resolution grid. After applying the proposed algorithm on USAF resolution chart, perceivable improvement in the contrast of resolution line pattern as compared to low resolution image is observed. © Anita Publications. All rights reserved.

Keywords: Multi frame super-resolution, Multi-aperture camera, ℓ_1 regularization, Super-resolution.

DOI: 10.54955/AJP.29.10-12.2020.853-862

1 Introduction

A multi-aperture imaging system like TOMBO [1-10] uses an array of micro-lenses to generate multiple images of a scene. These images share the space-bandwidth product offered by the imaging sensor. If we consider the multi-aperture system to have been derived from a single aperture system by replacing the single lens with an array of micro-lenses (with the same F#), there is a reduction in the system volume due to smaller focal-length of the micro-lenses leading to a more compact system. Since the multiple imaging channels share the space-bandwidth product of the sensor, the digital images generated by each channel has a lower resolution as compared to that generated by an equivalent single aperture imaging channel. This necessitates the scaling up of the image with a view to restoring the original resolution.

Scaling up an image using conventional interpolation techniques does not help in improving resolution as the information content in the image remains the same. One of the approaches to scale up an image with enhanced resolution is to use multiple images shifted relative to each other by a fraction of the detector pixel pitch. The generic class of algorithms that are capable of reconstructing a scaled-up image with a higher resolution from multiple sub-pixel shifted images are referred to as 'Multiframe Super-resolution' (MFSR) techniques [11-29]. An alternate approach to Super-resolution is to generate a high-resolution image

---

Corresponding author
e mail: unni@irde.drdo.in (Unnikrishnan Gopinathan)

from a single low-resolution image using a dictionary referred to as Single Image Super-resolution technique. Neural Network techniques have been used to learn the dictionary [30-34].

Super-resolution image reconstruction [35] is an inverse problem [36-38], the solution of which requires the understanding of the forward imaging model that accurately describes the physical formation of Low Resolution (LR) images from the hypothetical High Resolution (HR) image. Figure 1(a) considers a simplistic imaging model where the HR image is assumed to undergo a shift and down-sampling operation to form the LR images. Under the assumption that image formation process is free of blur and noise degradations and the shifts are accurate and known *a priori*, an error free HR image reconstruction is possible with an up-sampling operation, and a shift-add operation applied to each LR image as shown in Fig 1(b). However, in a real-world situation, the image undergoes degradations mainly due to limited aperture size of the optics and noise present in the imaging system resulting in a loss of information. The shifts that the HR image undergoes are random in nature and seldom known. In a real-world situation, one is required to estimate these shifts from noisy and blurred LR images. All the above reasons make the ill-posed problem of Super-resolution image reconstruction an extremely challenging one.

The success of MFSR techniques depends to a large extent on (i) the presence of subpixel shift in the LR images, the accurate determination of these shifts and the use of these shifts to interpolate to a higher resolution grid to obtain a scaled-up HR image (ii) the mathematical model that represents the forward image formation process incorporating the various degradations in the imaging channel. Though it is generally accepted that accurate modeling of the imaging channel degradations has a direct bearing on the quality of image reconstruction, the computing requirements and the complexity of the mathematical models are also important considerations. Depending on the a priori information available, the degradation function may be assumed to be known or unknown. For the latter cases, blind deconvolution techniques may be used.

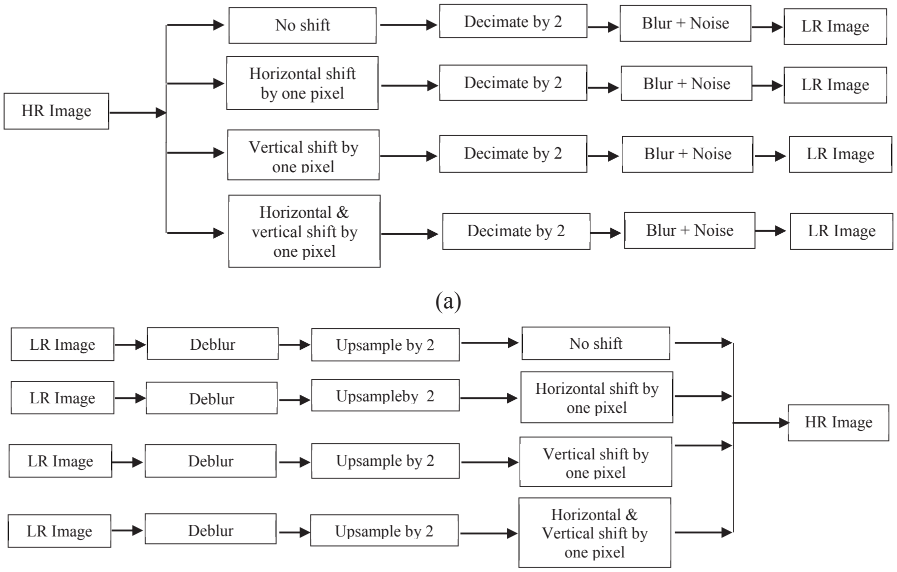

(a)

(b)

Fig 1. (a) Forward model of image formation that forms basis for proposed multiframe super resolution image reconstruction algorithm (b) Inverse model for HR image reconstruction.

Our approach to the scaling up images involves the following steps as shown in Fig 1(b) - (i) deblurring the noisy LR images, (ii) estimating the subpixel shifts, (iii) up-sampling the images, (iv) Shift and Add. This would correspond to the mathematical model shown in Fig 1(a) where blurring and noise addition happens after the decimation operation on the LR images. This is different from the earlier approaches where the deblurring is done on the estimated HR image. The advantages of our approach are the following: (1) the shift estimation is done on the deblurred image which is more accurate. (2) The deblurring operation is done separately for each channel giving more flexibility for addressing the degradations of each channel separately. We use two well-known algorithms for deblurring – FISTA [39] and SALSA-based [40-41] on ℓ_1 regularization.

Let the N outputs of an N-channel imaging system be denoted as $Z_1,....,Z_N$ each with $M_1 \times M_2$ pixels. It is required to reconstruct an HR image scaled up by a factor r with $rM_1 \times rM_2$ pixels, where $r \le \sqrt{N}$. The scaled-up image will have an equivalent resolution obtained from a single aperture imaging system having optics of same F# and a detector with $rM_1 \times rM_2$pixels and pixel pitch $p_x/r \times p_y/r$, respectively.

Deblur using FISTA

Let blur PSF of the k^{th} channel be represented as blurring matrix A_k.The formation of blurred image from exact image is given by

$$\boldsymbol{z}^{\boldsymbol{k}} = A_k x^{\boldsymbol{k}} + \boldsymbol{n}_{\boldsymbol{k}} \text{ , } k = 1\dots N \tag{1}$$

where A_k is the matrix representation of blurring function, $\boldsymbol{z}^{\boldsymbol{k}}$ is vector representation of blurred image Z_k and $\boldsymbol{x}^{\boldsymbol{k}}$ is vector representation of the two-dimensional image X_k expressed in the matrix form. $\boldsymbol{n}_{\boldsymbol{k}}$ is the additive noise in the k^{th} channel. In the absence of noise, the estimate of $\boldsymbol{x}^{\boldsymbol{k}}$ based on Least Square (LS) approach gives

$$\hat{x}^k = \arg\min_{x^k} \|z^k - A_k x^k \|^2 \tag{2}$$

The ill-posed nature of inverse problem requires choosing solution that is close to the accurate estimate $\boldsymbol{x}^{\boldsymbol{k}}$ given the infinite possible solutions possible from noisy ill-conditioned observations. Regularization term helps converting inverse problem from ill-posed to a well posed one. Adding a regularization term to the above solution in Eq (2) gives

$$\hat{x}^k = \arg\min_{x^k} \|z^k - A_k x^k\|^2 + \lambda\Theta(x^k) \tag{3}$$

$\Theta(..)$ denotes a convex regularizer and $\lambda > 0$ is a regularization parameter that providesa trade-off between fidelity to measurements and noise sensitivity. A natural image is sparse in orthogonal basis such as Wavelet basis. This knowledge can be used to incorporate the ℓ_1 norm of Wavelet coefficients in the regularization term to give $\Theta(x^k) = \|W\alpha^k\|_1$, where W denotes inverse Wavelet transform, α^k is a sparse vector containing Wavelet coefficients corresponding to x^k. The Eq (3) can be rewritten as

$$\hat{\alpha}^k = \arg\min_{\alpha^k} \|z^k - A_k \alpha^k\|^2 + \lambda\|\alpha^k\|_1 \tag{4}$$

The presence of the ℓ_1 term is used to induce sparsity in the optimal solution $\hat{\alpha}^k$. For deblurring applications, A is chosen as $A = RW$, where R is blurring matrix and W contains Wavelet basis (multiplying by W corresponds to inverse Wavelet Transform). Since most applications like image deblurring involves dense matrix data which precludes use of methods which requires matrix explicitly stored. The search for cheap matrix vector multiplication such as FFT, DCT ends on simple gradient based methods where dominant computational effort is on cheap matrix vector multiplication involving A and A^T.

One of the most popular methods for solving problem given by Eq (4) is in the class of iterative shrinkage thresholding algorithms (ISTA), where each iteration involves matrix-vector multiplication with A and A^T followed by shrinkage/soft threshold step. ISTA solves a class of optimization problem that can be formulated as

$$\text{Min}_x \; \{ f(\boldsymbol{x}) + g(\boldsymbol{x}) \} \tag{5}$$

where $f, g: \mathbb{R}^n \rightarrow \mathbb{R}$. g is a continuous convex function which can be non-smooth and f is a smooth convex function that is continuously differentiable with a Lipschitz continuous gradient L(f). ISTA solves the minimization problem as

$$x_m = \arg\min_x \left\{ g(x) + \frac{L}{2} \| x - \left(x_{m-1} - \frac{1}{L} \nabla f(x_{m-1}) \right) \|^2 \right\} \tag{6}$$

where $L = L(f)$ is a Lipschitz constant of ∇f plays the role of step size. $\boldsymbol{x}_{\boldsymbol{m}}$ is the estimate of $\boldsymbol{x}$ in the m^{th} step.

FISTA is an improvement of ISTA. FISTA not only preserves efficiency of the original ISTA but also promotes effectiveness of ISTA so that FISTA can obtain global convergence. In FISTA algorithm, the estimate in the m^{th} step is $\boldsymbol{x_m}$ is

$$x_m = \arg\min_x \left\{ g(x) + \frac{L}{2} \| x - (1+\xi)\left(x_{m-1} - \frac{1}{L}\nabla f(x_{m-1})\right) - \xi\left(x_{m-2} - \frac{1}{L}\nabla f(x_{m-2})\right) \|^2 \right\} \tag{7}$$

where $\xi = 2\left(\frac{t_{m-1} - 1}{1 + \sqrt{1 + 4\,t_{m-1}^2}}\right)$, t_{m-1} being the step size in the (m-1)th step.

For $f(\boldsymbol{x}) = \|A\boldsymbol{x} - \boldsymbol{b}\|^2$ and $g(\boldsymbol{x}) = \|x\|_1$, $\boldsymbol{x_m}$ in Eq 6 is estimated using a shrinkage/soft threshold step given by

$$\boldsymbol{x_m} = (1+\xi)\,\wp_{\lambda/L}\,(x_{m-1}) - \frac{2}{L}A^T(Ax_{m-1} - b) + \xi\wp_{\lambda/L}\left(x_{m-2} - \frac{2}{L}A^T(Ax_{m-2} - b)\right) \tag{8}$$

where the soft threshold operator $\wp_\tau(\boldsymbol{.})$ is defined as

$$\wp_\tau(x) = \begin{cases} x & \text{if } x > \tau \text{ or } x < -\tau \\ 0 & \text{if } -\tau \le x \le \tau \end{cases}$$

The soft threshold operator $\wp_\tau(\boldsymbol{.})$ acts on each element of the vector **x**.

When $\mathbf{x} = \boldsymbol{\alpha}^{\mathbf{k}}$, $A = A_k$ and $\mathbf{b} = \mathbf{z}^{\mathbf{k}}$, the above equation can be written as

$$\boldsymbol{\alpha}_{\boldsymbol{m}}^{\boldsymbol{k}} = (1+\xi)\,\wp_{\lambda/L}\,(\boldsymbol{\alpha}_{\boldsymbol{m}-1}^{\boldsymbol{k}}) - \frac{2}{L}A_k^T(A\boldsymbol{\alpha}_{\boldsymbol{m}-1}^{\boldsymbol{k}} - b)) + \xi\wp_{\lambda/L}\,(\boldsymbol{\alpha}_{\boldsymbol{m}-2}^{\boldsymbol{k}} - \frac{2}{L}A_k^T(A\boldsymbol{\alpha}_{\boldsymbol{m}-2}^{\boldsymbol{k}} - b)) \tag{9}$$

In image deblurring problem PSF is having double symmetry (reflexive boundary conditions) and therefore blurring matrix A is symmetric implies that $A^T = A$ and this simplifies calculations.

Deblur using SALSA

An alternate approach to solve the inverse problem in Eq (1) is to solve the constrained optimization problem of the form,

$$\min \Theta(x) \; \textit{subject to} \; \| \boldsymbol{z^k} - A^k \boldsymbol{x^k} \|_2 \le \varepsilon \tag{10}$$

where $\Theta(x)$ is the regularizer and $\varepsilon < 0$ is a parameter which depends upon the noise variance. For $\Theta(x) = \|x\|_1$, this problem is known as Basis Pursuit denoising (BPD) [40] and is solved using C-SALSA algorithm [40,41]. The constrained problem is transformed into an unconstrained one by adding the indicator function of the feasible set, the ellipsoid:

$$E(\varepsilon, A^k, \boldsymbol{z^k}) = \{\boldsymbol{x^k} \in R^n : \|\boldsymbol{z^k} - A^k x^k\|_2 \le \varepsilon\} \tag{11}$$

Therefore, constrained problem Eq (10) can be written as an unconstrained problem:

$$\min_{u \in R^d}(g_1(H^1u) + g_2(H^2u)) = \min \Theta(\boldsymbol{x^k})_{u \in R^d} + I_E(\varepsilon, I, z^k)(A^k \boldsymbol{x^k}) \tag{12}$$

$\varepsilon > 0$ is a parameter which depends on noise variance. By application of variable splitting above unconstrained problem is converted to different constrained problem and finally is dealt with using the ADMM technique. Moreau proximal mapping required in ADMM technique for $g_1 = \Theta = \|x\|_1$ is soft threshold operator

$$prox_{\lambda\tau}(\boldsymbol{x^k}) = max\left(0, 1 - \frac{\tau}{|\boldsymbol{x^k}|}\right)\boldsymbol{x^k} \tag{13}$$

τ is threshold for soft threshold operator.

2 Result and Discussion

Simulation Results

The algorithm was tested on four sub-pixel shifted blurred and noisy low resolution images. These images were generated from a 256 × 256 pixel by giving shifts in three directions- one pixel shift to the right, one pixel shift in the upward direction, one pixel shift to right and upward direction- and thereby creating four shifted images with shifts (0,0), (0,1), (1,0), (1,1). Then each image was down-sampled by factor 2 and a Gaussian blur of size 3×3 and standard deviation 4 was applied using the MATLAB functions *imfilter* and *f special* followed by an additive zero mean white Gaussian noise with standard deviation 0.01. The original and one of the four LR image is shown in Fig 2(a) and (b), respectively.

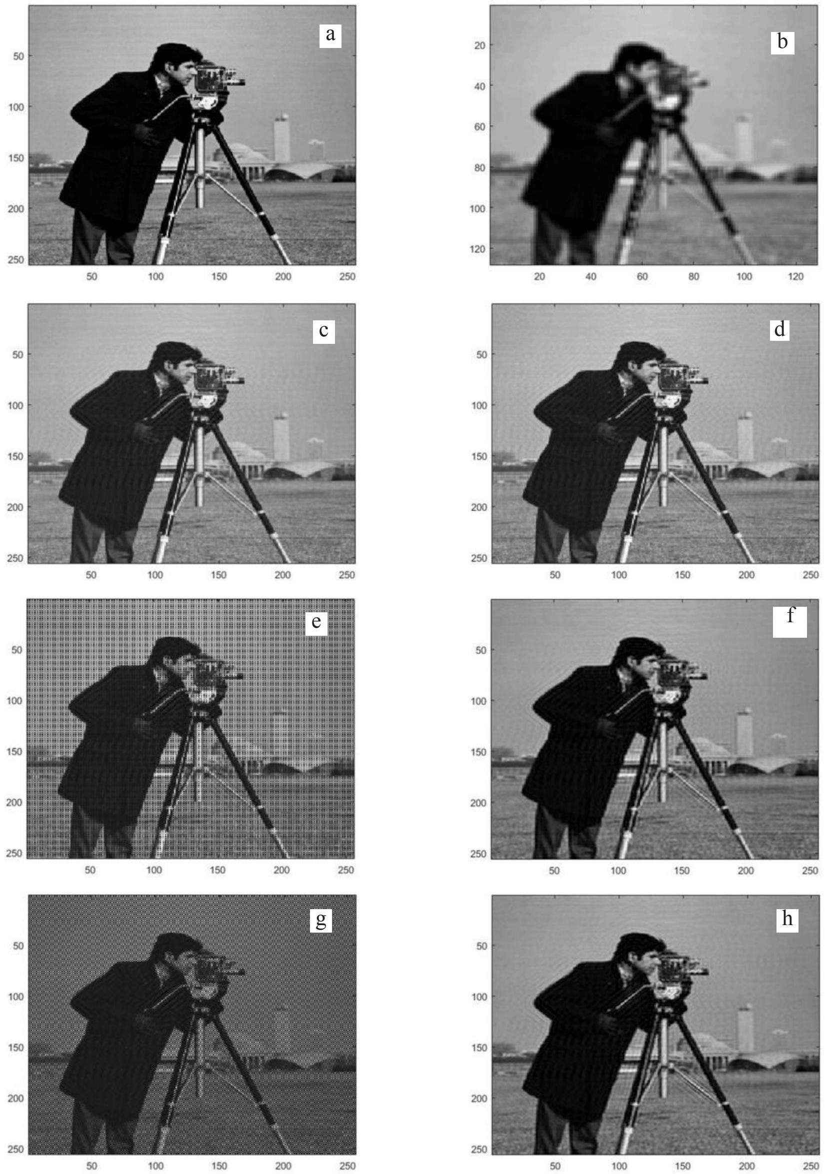

Fig 2. (a) Original Cameraman image (b) Blurred and noisy LR image (c) HR image reconstructed with FISTA for deblurring (d) HR image reconstructed with SALSA for deblurring (e) HR reconstructed image with three subpixel shifted LR images (one subpixel shifted LR image is missing) using FISTA for deblurring (mean square error = 0.2625) (f) HR reconstruction after applying filter to image in (e) (mean square error = 0.1365) (g) HR reconstructed image with two subpixel shifted LR images (two subpixel shifted LR image are missing) using FISTA for deblurring (mean square error = 0.3706) (h) HR reconstruction with after applying filter to image in (g) (mean square error = 0.264).

HR image in Fig 2(c) and (d) are reconstructed by applying the proposed algorithm. Figure 2(c) was reconstructed with deblur as intermediate step by assuming reflexive boundary conditions and applying FISTA algorithm for deblurring by solving lasso problem, where $\boldsymbol{z}^{\boldsymbol{k}}$ is vector representation of observed image Z_k and $A = RW$, where R is blurring matrix representing the blur operator and W is inverse of a eight level Haar Wavelet Transform. The regularization parameter was tuned to be $\lambda = 0.097$ which corresponds to least MSE over range of values and the initial image was the blurred image. The Lipschitz constant was computable since the eigen values of the matrix $\mathrm{A}^{\mathrm{T}}\mathrm{A}$ can be calculated using 2D-cosine transform. The number of iterations were 113.

Figure 2(d) was reconstructed by proposed algorithm with deblur as intermediate step by assuming periodic boundary conditions and applying SALSA algorithm for deblurring by solving constrained minimization problem in Eq (12), where **b** is vector representation of observed image and R is blurring matrix [42]. The ϵ parameter that depends on noise variance was chosen to be 4.6. The parameter τ is the threshold for soft threshold operator which was chosen to be 2×10^{-4}. These parameters were tuned so that least MSE between original image and estimated image was obtained. The number of iterations were 113.

Mean-square-error between original image and estimated image is less for HR image with SALSA for deblurring than HR image with FISTA for deblurring, also computational time is less for former case with same number of iterations. The same experiment was performed for five other blur and noisy LR images. As blur increased, MSE also increased in both cases, while HR reconstruction with FISTA for deblurring performs better than other method as noise deviation is increased. Furthermore, as blur and noise in the image increases computational time required for HR reconstruction is also more.

Table 1. Comparison of HR reconstruction methods with SALSA and FISTA algorithms used for deblurring

	Blur PSF	Noise Deviation	Optimum Parameter Value	Mean Square Error	No of Iterations	Computational Time (seconds)
SALSA	3×3	0.01	$\tau = 0.0069$ $\epsilon = 0.0046$	0.0181	113	3.2834
		0.1	$\tau = 0.0099$ $\epsilon = 5\text{-}5.2$	0.0192	113	3.3044
		1	$\tau = 0.93$ $\epsilon = 16$	0.0481	113	3.2438
	5×5	0.01	$\tau = 0.00037$ $\epsilon = 6.1$	0.0304	113	3.2789
		0.1	$\epsilon = 0.00037$ $\epsilon = 6$	0.0319	113	3.2785
		1	$\tau = 0.5$ $\epsilon = 19$	0.0686	113	3.5757
FISTA	3×3	0.01	$\lambda = 0.097$	0.0189	113	6.2353
		0.1	$\lambda = 0.043$	0.0190	113	6.2541
		1	$\lambda = 0.99$	0.0457	113	6.3118
	5×5	0.01	$\lambda = 0.0033$	0.0343	113	6.1624
		0.1	$\lambda = 0.095$	0.0349	113	6.3220
		1	$\lambda = 3$	0.0493	113	6.2159

In practice, not all the four sub-pixel shifted images are available for reconstruction. When one of the four sub-pixels shifted image is missing artifacts are observed as shown in Fig 2(e), as on a higher sampling grid corresponding samples are missing. To remove these artifacts low pass filter with 50 pixels mask in Fourier domain was applied which resulted in HR image as shown in Fig 2(f). When two sub-pixel shifted images are missing artifacts are observed as shown in Fig 2(g) which were then removed by applying low pass filter with 50 pixels mask in Fourier domain shown in Fig 2(h). However, MSE between original image and reconstructed image is now increased to a higher value.

Experimental Results

A. *System Configuration*

The algorithm was tested on a multi-aperture camera with the following configuration. The optics comprised of a 5×5 array of micro-lenses. Each lens has diameter of 0.8 mm and focal length of 4 mm. The distance between lens array and CMOS sensor was 4 mm. CMOS sensor had 1024 × 1280 pixels and pixel pitch equal to 5.2 µm × 5.2 µm.

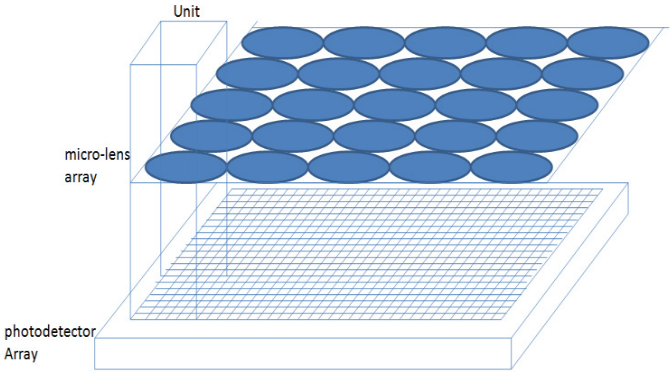

Fig 3. System configuration

B. *Image Preprocessing*

The raw image was segmented into 25 images each with size of 100×100 pixels. Any shift between these 25 segmented images that corresponds to an integer multiple of one pixel is estimated by a correlation operation [43] between one of the images (the first image of the array) taken as the reference and the other images. The images are corrected for these shifts so that what remains is sub-pixel shift which we use in the MFSR algorithm.

C. *Experimental Results*

The results obtained for a USAF resolution chart that was placed at distance of 6 cm from the camera are shown in Fig 4. Figure 4(a) shows the frame captured by multi-aperture camera. There are 25 LR images each with size 100×100. Figure 4(b) shows LR image corresponding to first lens interpolated by factor of 2 using bicubic interpolation (thus size 200×200). Figure 4(c) shows HR image scaled up by factor 2 that is estimated by algorithm proposed in this paper. We started with deblurring each image by assuming blur PSF to be Gaussian of size 3×3 and standard deviation 0.45. We perform deconvolution using FISTA algorithm with W chosen as inverse of 8 level Haar Wavelet transform. Regularization parameter was chosen to be $\lambda = 3.1\times10^{-7}$. As blur PSF is symmetric, we have reflexive boundary conditions on blurring matrix R. Thus, Eigen values of A can easily be computed using 2-dimensional discrete cosine transform [42] and therefore Lipschitz constant was computed as Eigen values of matrix A^TA. Iterations are chosen to be 200. Then to find shift between images with respect to reference image (first image of the array) each deblurred image was interpolated and shift was found by correlation method. It was found that only three sub-pixel shifted images were available for reconstruction with (1,0) shifted image missing. After recording the shifts as third step, each deblurred image was up-sampled on higher sampling grid and then shifted back and added to get HR image. As one subpixel shifted image is missing corresponding samples on higher sampling grid are missing, thus HR with artifacts is observed as shown in Fig 4(c). By applying low pass filter of 50×50 pixels mask in Fourier domain HR image as shown in Fig 4(d) is obtained.

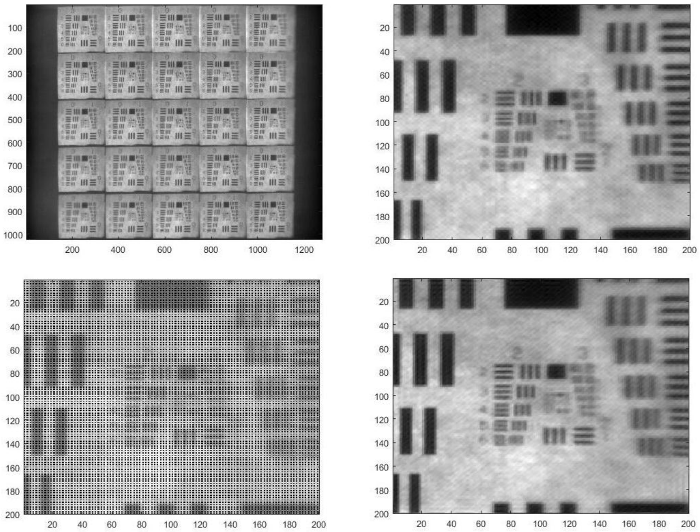

Fig 4. Clockwise from top right (a) A frame grabbed with multi-aperture camera of size 1024×1280 pixels (b) Interpolated LR image corresponds to first lens in array (c) HR image reconstructed with three subpixel shifted LR images (0,0),(0,1),(1,0) (one subpixel shifted LR image is missing) (d) HR image reconstructed with three subpixel shifted images and applying filter.

The modulation transfer function [44] for each horizontal and vertical line pattern which corresponds to resolution in lines per mm is shown in Fig 5(a) and (b), respectively. There is perceivable improvement in the contrast of resolution of horizontal line pattern as compared to low resolution image.

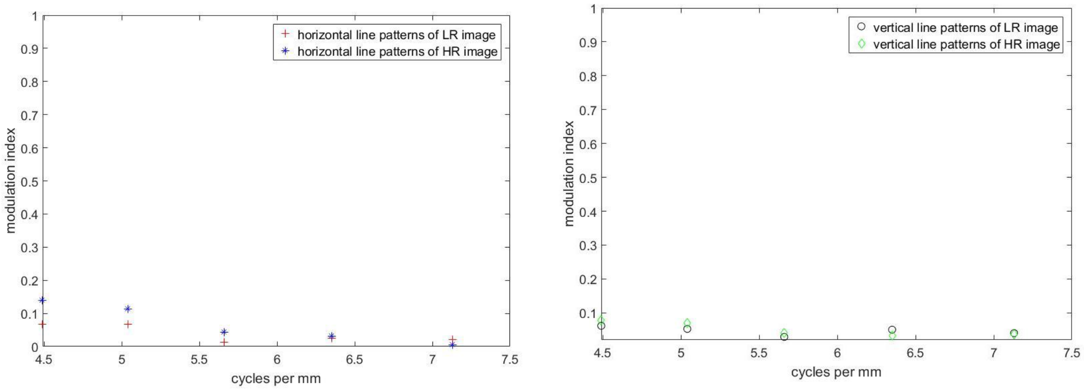

Fig 5. (a) Modulation transfer function v/s resolution in cycles per mm for horizontal line pattern on resolution chart (b) Modulation transfer function v/s resolution in cycles per mm for vertical line pattern on resolution chart.

A 'No reference Image quality metric' defined in the frequency domain [45] was used to compare the HR image with LR image. The metric was calculated as follows: The 2-D Fourier Transform of the image is performed. The Image quality metric in the Fourier domain is determined by finding the number of pixels that has the absolute value of the Fourier Transform greater than a threshold value normalized by the total number of pixels. The threshold is chosen as the 1/1000 of the maximum value of the absolute value of Fourier transform. The Frequency domain Image quality metric effectively determines the spread of the Fourier spectrum. The Fourier spectrum spread will be more if the image has higher spatial frequency content. The thresholding operation makes the metric less sensitive to noise as compared to other spatial domain image quality metric like Variance. The values of the Fourier domain Image quality metric of the LR image and the HR image were estimated to be 0.0242 and 0.0256, respectively.

3 Conclusion

We apply robust reconstruction techniques based on FISTA and C-SALSA algorithms to reconstruct the HR image from multiple LR images in a multi-aperture camera. Images obtained from a multi-aperture camera have low SNR associated with it due to its small aperture optics. Also, multiple channels have different point spread functions. We first deblur the LR image using the ℓ_1 regularization methods based on FISTA and C-SALSA. In next step, the shifts between deblurred images is estimated. Deblurred LR images are then scaled up on HR image grid. For HR image reconstruction shift and add operation is performed on LR images. We present simulation and experimental results that show perceptible improvement in the resolution of high-resolution image as compared to the low resolution image. It is hoped that many of the recent advances in signal processing will lead to considerable performance enhancement of computational imaging systems like TOMBO camera.

References

1. Tanida J, Kumagai T, Yamada K, Miyatake S, Ishida K, Morimoto T, Kondou N, Miyazaki D, Ichioka Y, Thin observation module by bound optics (TOMBO): concept and experimental verification, *Appl Opt*, 40(2001)1806–1813.
2. Kitamura Y, Shogenji R, Yamada K, Miyatake S, Miyamoto M, Morimoto T, Masaki Y, Kondou N, Miyazaki D, Tanida J, and Ichioka Y, Reconstruction of a high-resolution imageon a compound-eye image-capturing system, *Appl Opt*, 43(2004)1719–1727.
3. Nitta K, Shogenji R, Miyatake S, Tanida J, Image reconstruction for thin observation module by iterative backprojection, *Appl Opt*, 45(2006)2893–2900.
4. Shankar M, Willett R, Pitsianis N P, Kolste R Te, Chen C, Gibbons R, Brady D J, Ultra-thin multiple-channel LWIR imaging system, *Proc SPIE*, 6294(2006)629411; doi.org/10.1117/12.681386.
5. Kanaev A V, Scribner D A, Ackerman J R, Fleet E F, Analysis and application of multi-framesuper-resolution processing for conventional imaging systems and lens-let arrays, *Appl Opt*, 46(2007)4320-4328.
6. Kanaev A V, Ackerman J R, Fleet E F, Scribner D A, TOMBO sensor with scene-independent super-resolution processing, *Opt Lett*, 32(2008)2855–2857.
7. Shankar M, Willett R, Pitsianis N, Schulz T, Gibbons R, Kolste R Te, Carriere J, Chen C, Prather D, and Brady D, Thin infrared imaging systems through multichannel sampling, *Appl Opt*, 47(2008)B1–B10.
8. Portnoy A D, Pitsianis N P, Sun X, Brady D J, Multichannel sampling schemes for optical imaging systems, *Appl Opt*, 47(2008)B76–B85.
9. Mendelowitz S, Klapp I, Mendlovic D, Design of an image restoration algorithm for the TOMBO system, *J Opt* Soc Am A, 30(2013)1193–1204.
10. Gao Y, Yang P, Tang G, Xu B, Ao M, Experimental resolution comparison between the TOMBO and single lens systems, Proc SPIE 9227(2014), 92270B.
11. Peleg S, Keren D, Schweitzer L, Improving image resolution using subpixel motion, *Pattern Recogn Lett*, 5(1987) 223–226.
12. Irani M, Peleg S, Improving resolution by image registration, *CVGIP: Graphical Models and Image Processing*, 53(1991)231–239.
13. Ur H, Gross D, Improved resolution from subpixel shifted pictures, *CVGIP: Graphical Models and Image Processing*, 54(1992)181–186.
14. Elad M, Feuer A, Restoration of a single super-resolution image from several blurred,noisy, and under-sampled measured images, *IEEE Trans Image Process*, 6(1997)1646–1658.
15. Hardie R, Barnard K J, Armstrong E E, Joint MAP registration and high-resolution image estimation using a sequence of under-sampled images, *IEEE Trans Image Process*, 6(1997)1621–1633.
16. Chiang M C, Boult T E, Efficient super-resolution via image warping, *Image Vis*, 18(2000)761–771.

17. Elad M, Hel-Or Y, A fast super-resolution reconstruction algorithm for pure translational motion and common space-invariant blur, *IEEE Trans Image Process*, 10(2001)1187–1193.
18. Nguyen N, Milanfar P, Golub G H, A computationally efficient image super-resolution algorithm, *IEEE Trans Image Process*, 10(2001)573–583.
19. Ng M, Bose N, Mathematical analysis of super-resolution methodology, *IEEE Signal Process Mag*, 20(2003)62–74.
20. Park S, Park M, Kang M G, Super-resolution image reconstruction: a technical overview, *IEEE Signal Process Mag*, 20(2003)21–36.
21. Farsiu S, Robinson M D, Elad M, Milanfar P, Fast and robust multi-framesuper-resolution, *IEEE Trans Image Process*, 13(2004)1327–1344.
22. Young S S, Driggers R G, Super-resolution image reconstruction from a sequence of aliased imagery, *Appl Opt*, 45(2006)5073-5085.
23. Shankar P M, Neifeld M A, Multi-framesuper-resolution of binary images, *Appl Opt*, 46(2007)1211–1222.
24. Ashok A, Neifeld M A, Pseudorandom phase masks for super-resolution imaging from subpixel shifting, *Appl Opt*, 46(2007)2256–2268.
25. Robinson M D, Stork D G, Joint digitaloptical design of super-resolutionmulti-frameimaging systems, *Appl Opt*, 47(2008)B11–B20.
26. Choi K, Schulz T J, Signal-processing approaches for image-resolution restoration for TOMBO imagery, *Appl Opt*, 47(2008)B104–B116.
27. Bishop T E, Favaro P, The Light field camera: Extended depth of field, aliasing, and super-resolution, *IEEE Trans Pattern Anal Mach Intel*, 34(2012)972–986.
28. Young S S, Driggers R G, Jacobs E L, Signal Processing and Performance Analysis for Imaging systems, (Artech House, Boston), 2008.
29. Milanfar P (Ed), Super Resolution Imaging, (CRC Press, Boca Raton), 2011.
30. He K, Zhang X, Ren S, Sun J, Deep residual learning for image recognition, Proc IEEE conf on Computer Vision and Pattern Recognition, (2016)770-778.
31. Dong C, Loy C C, He K, Tang X, Image super-resolution using deep convolutional networks, *IEEE Trans Pattern Anal Mach Intel*, 38(2016)295–307.
32. Kim J, Kwon J, Lee K M, Accurate image super-resolution using very deep convolutional networks, Proc IEEE conf on Computer Vision and Pattern Recognition (CVPR), (2016)1646–1654.
33. Lim B, Son S, Kim H, Nah S, Lee K M, Enhanced deep residual networks for single image super-resolution, IEEE conf on Computer Vision and Pattern Recognition (CVPR) Workshops, (2017)136–144.
34. Tai Y, Yang J, Liu X, Image Super-resolution via deep recursive residual network, IEEE conference on Computer Vision and Pattern Recognition (CVPR), (2017)3147–3155.
35. Candes E J, Fernandez-Granda C, Towards a mathematical theory of Super-resolution, *Commun Pure Appl Math*, 67(2014)906-956.
36. Bertero M, Boccacci P, Introduction to inverse problems in imaging, (CRC Press) 1998.
37. Barrett H H, Myers K J, Foundations of Imaging Science, (Wiley,)2003.
38. Jin K H, McCann M T, Froustey E, Unser M, Deep convolutional neural network for inverse problems in imaging, *IEEE Trans Image Process*, 26(2017)4509-4522.
39. Beck A, Teboulle M, A fast iterative shrinkage-thresholding algorithm for linear inverse problems. SIAM J Imaging Sciences, 2(2009)183–202.
40. Afonso M V, Bioucas-Dias J M, Figueiredo M A, Fast image recovery using variable splitting and constrained optimization, *IEEE Trans Image Process*, 19(2010)2345–2356.
41. Afonso M V, Bioucas-Dias J M, Figueiredo M A, An augmented Lagrangian approach to the constrained optimization formulation of imaging inverse problems, *IEEE Trans Image Process*, 20(2011)681–695.
42. Hansen P C, Nagy J G, O'Leary D P, Deblurring Images: Matrices, Spectra, and Filtering, (Society for Industrial and Applied Mathematics, Philadelphia). 2006.
43. Guizar-Sicairos M, Thurman S T, Fienup J R, Efficient subpixel image registration algorithms, *Opt Lett*, 32(2008)156-158.
44. Goodman J W, Introduction to Fourier Optics, 3rd edn, (Roberts and Company Publ), 2016.
45. De K, Masilamani V, Image sharpness measure for blurred images in frequency domain, *Procedia Engineering*, 64(2013)149–158.

[*Received*: 15.11.2020; *accepted*: 19.12.2020]